Peculiarity and defect structure of the natural and synthetic zeolite mordenite: A single-crystal X-ray study

PETRA SIMONCIC AND THOMAS ARMBRUSTER*

Laboratorium für Chemische und Mineralogische Kristallographie, University of Bern, Freiestrasse 3, CH-3012 Bern, Switzerland

ABSTRACT

Single-crystal X-ray data were collected from a natural fibrous mordenite crystal of composition $K_{2.99}Ca_{1.85}Na_{1.06}Al_{7.89}Si_{40.15}O_{96} \cdot 28H_2O$ and from a platy synthetic mordenite crystal of composition $Na_6Al_{6.02}Si_{42.02}O_{96} \cdot 19H_2O$. Diffraction data were measured with a point detector using a sealed X-ray tube and an image plate using synchrotron radiation, respectively. Both structures exhibit the same defect features visible in difference-Fourier maps. Domains of the entire *Cmcm* framework structure are reproduced by a non-crystallographic (001) mirror plane at $z = 0$ and $z = 1/2$. An identical description is a shift of framework domains 1/2 along the **c** axis. The concentration of this defect domain is 2.7(2) and 3.1(1)% for the natural and synthetic mordenite crystals, respectively. Reproductions of reciprocal layers from synchrotron image-plate data reveal diffuse scattering for *hkl* layers with $l = 2n + 1$. The diffuseness of these layers is not homogeneous but concentrates in the form of halos around selected reflections allowed for *C*-centering. Diffuse features in electron diffraction patterns of natural and synthetic mordenite have been described before and were interpreted either as evidence of $c/2$ faults or intergrowth with different mordenite-related structure-types. We have modeled a (100) defect layer that is modified from the mordenite characteristic puckered sheet of six-membered rings and allows coherent intergrowth of identical structural subunits shifted by $c/2$. These defect domains do not influence or obstruct the 12-membered ring-channels characteristic of this zeolite. The major difference in Si,Al distribution between the two samples is that the natural crystal has Al strongly enriched at T3, which is part of the four-membered rings. We suggest that a synergetic effect between extraframework cations and Si, Al ordering during crystal growth is responsible for Al enrichment in natural mordenite with ca. 2 Ca p.f.u. close to T3.

INTRODUCTION

Mordenite is one of the most siliceous natural zeolites. It has an orthorhombic unit cell of topological space-group symmetry *Cmcm* ($a = 18.13$, $b = 20.5$, $c = 7.52$ Å) with idealized chemical composition $Na_8Al_8Si_{40}O_{96} \cdot 24H_2O$. The structure of mordenite can be described as composed of edge-sharing five-membered rings of tetrahedra (secondary building unit 5-1) forming chains along **c** (Meier 1961). However, the mordenite framework can also be more comprehensibly envisioned as composed of puckered sheets parallel to (100), made up of six-membered rings of tetrahedra (Meier 1978; Armbruster and Gunter 2001). These sheets are interlinked by four-membered rings (Fig. 1) such that large, ellipsoidal 12-membered (12MRc: aperture 7×6.5 Å) and strongly compressed eight-membered rings (8MRc: aperture 5.7×2.6 Å) define channels parallel to **c**. Another set of compressed eight-membered rings (8MRb: aperture 3.4×4.8 Å) connects the wide channels with strongly compressed channels parallel to **b**. At least for large extraframework ions and molecules mordenite has only a one-dimensional channel system for diffusion (Terasaki et al. 1988). The eight-membered ring channels, running along **b**, which emerge from the wide tubes are staggered at the intersection with the strongly compressed channels (aperture 5.7×2.6 Å) before they end again in the wide tubes (Fig. 2). Extraframework cations in mordenite mainly occupy three sites. Two of these sites are close to the four-membered rings and are

located in the connecting channels parallel to **b**. Another cation position is located at the center of the main 12-membered ring channel (e.g., Armbruster and Gunter 2001).

Natural mordenite occurs in rather large quantities in some altered vitreous tuffs. It has a characteristic fibrous habit and if finely crystalline it may be added to the group of asbestiformous minerals causing lung diseases (Lilis 1981; Stephenson et al. 1999).

Mordenite is also synthesized in large quantities, mainly for industrial application as a catalyst. From a technical point of view two different varieties of mordenite are distinguished (Sand 1968). Large-port mordenite exhibits the properties predicted for a zeolite with accessible 12-membered ring channels: (1) molecules with a diameter >4.5 Å can be introduced into the large channels; (2) the NH_4^-- and H-exchanged forms are able to crack significant amounts of hexane at 450 °C. Large-port mordenite is hydrothermally synthesized in the Na-form between 75 and 260 °C. Small-port mordenite accepts only molecules with a diameter <4.2 Å and is thus less favorable for industrial applications. Small-port mordenites are usually obtained under hydrothermal synthesis conditions between 275 and 300 °C (Sand 1968). In addition, most natural mordenites have properties characteristic of small-port mordenite. There are chemical recipes for transforming a small-port mordenite into the large port variety and vice versa (Sand 1968; Raatz et al. 1985). The reasons for small- and large-port behavior are controversial. The following hypotheses have been put forward: (1) location of extraframework cations, (2) the presence of amorphous material

---

* E-mail: thomas.armbruster@krist.unibe.ch
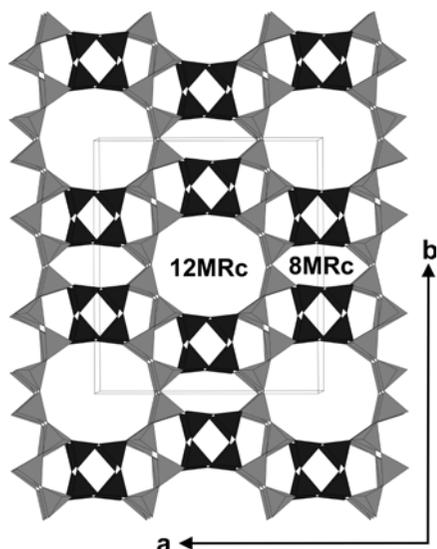
FIGURE 1. Tetrahedral framework structure of mordenite with unit-cell outlines. The structure is composed of puckered sheets (light gray shading) parallel to (100) formed by six-membered rings of tetrahedra (Meier 1978). These sheets are connected along **b** by four-membered ring pillars (dark gray shading) in such a way that 12-membered ring channels (12MRc) and compressed eight-membered ring channels are formed, both extending along **c**.
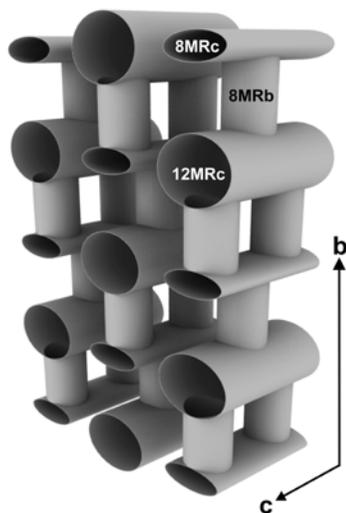
FIGURE 2. "Plumbing system" in mordenite accessible for extraframework-cation and -molecule diffusion. Notice that there is no straight connection between adjacent 12MRc tubes. The linking 8MRb tubes are staggered at the join with the strongly compressed 8MRc tubes. Thus for diffusion of large ions or molecules the structure of mordenite offers only one-dimensional passageways.

plugging the structural windows, and (3) stacking faults disrupting the continuity of the large channels. In particular the latter argument has been widely accepted for the varying properties of mordenite (Raatz et al. 1985).

There is a striking difference in morphology between the natural (fibrous) and the synthetic (platy) mordenite samples. Hamidi et al. (2001) suggest, based on a series of hydrothermal growth experiments, that the alkalinity of the system is the main factor influencing the crystal morphology. At low alkalinity platy crystals are formed whereas at higher alkalinity the crystals become more prismatic. On the other hand, Sano et al. (2001) were able to change the morphology of mordenite grown under corresponding conditions by addition of different aliphatic alcohols (methanol – 1-decanol), which were not incorporated into the zeolite channel-system. The morphological aspects are important for technical applications. The dominant (001) faces of platy mordenite enable easy access to the large 12-membered ring channels. Long prismatic or fibrous (along **c**) crystals have fewer large-channel openings and diffusion will be more sluggish. It seems that morphology is an additional parameter influencing small-port and large-port behavior.

Even though the crystal structure of mordenite was solved in the early sixties (Meier 1961) and much work has been done in this field since then, several questions still exist. Problems such as pseudo-centrosymmetry, Si,Al ordering, extraframework cation distribution, framework defects, faulting, and diffuse scattering have been addressed by several authors.

Pseudo-centrosymmetry

The first structural refinements were carried out with an Na-exchanged, natural mordenite in space group *Cmcm* (Meier 1961), but lower, acentric symmetry was already supposed due to Si,Al ordering and a suspicious T-O-T angle of 180°. Structure models of different symmetry, coherently intergrown with each other, were suggested yielding two different Si,Al conformations of the four-membered rings (Gramlich-Meier 1981). Although the Si,Al framework showed strong pseudo-centrosymmetry, the extraframework cation-distribution pointed to an acentric arrangement (Alberti et al. 1986). Symmetry lowering from *Cmcm* to C*mc*2_1 prevented the energetically unfavorable 180° T-O-T angle that appeared in the *Cmcm* refinement, and led to a better description of the extraframework cation-distribution.

Although characterization of the mordenite structure was highly improved by the acentric space group C*mc*2_1, refinement in the centric space group *Cmcm* is still applied in many crystallographic studies involving the mordenite structure (Shiokawa et al. 1989; Rudolf and Garcés 1994).

Framework defects and diffuse scattering

Crystallographic faulting in mordenite has been discussed by several authors either on a theoretical basis or by applying electron and X-ray diffraction methods. The reasoning of most studies of this type is to understand the enigmatic small- and large-port behavior of mordenite.

Kerr (1963) suggested a hypothetical structure of space-group symmetry *Immm*, closely related to mordenite, but of distinct topological symmetry due to the different heights of the four-membered rings of tetrahedra along the **c** axis. The field of hypothetical structures related to mordenite was elaborated by Sherman and Bennett (1973), who predicted additional structures of *Cmmm* and *Imcm* symmetry where the four-membered rings are attached at different levels along **c**. In all of these hypothetical structures the 12- and strongly compressed eight-membered ring channels run along **c** at the same position as in *Cmcm* mordenite. The same authors interpreted X-ray powder patterns of

synthetic and natural mordenites to show the dominant effect of the normal *Cmcm* structure of mordenite with subordinate intermingled *Cmmm*, *Immm*, and *Imcm* structures. Electron diffraction patterns of mordenite from Challis Valley, Idaho, showed streaks in *h0l* section where the streaks were occasionally decorated with diffuse maxima interpreted as intergrowths of *Cmcm*, *Cmmm*, *Immm*, and *Imcm* structures (Sherman and Bennett 1973). Crystals of the hypothetical *Cmmm*, *Immm*, and *Imcm* structures have never been found in synthetic products or in nature. Meier (1978) argued that the above hypothetical structures lack the puckered (100) sheet formed by six-membered rings of tetrahedra. These sheets are characteristic of mordenite-group zeolites comprising also dachiardite, epistilbite, ferrierite, and bikitaite (e.g., Armbruster and Gunter 2001).

Electron diffraction experiments on natural and synthetic mordenite (Sanders 1985) showed that there are layers of diffuse scattering perpendicular to $\mathbf{c}^*$ restricted to planes with Bragg indices $l = 2n + 1$ where the scattering is concentrated around reciprocal *hkl* lattice points allowed for *C*-centering for which $h + k = 2n$ (e.g., 111, 311, 511). The intersection of the Ewald sphere with the diffuse layers produces the continuous streaks in the *h0l* section discussed by Sherman and Bennet (1973). The electron diffraction results (Sanders 1985) were interpreted to be caused by linear faults parallel to the $\mathbf{c}$ axis which is the direction of the major channels. However, there was no indication of stacking faults normal to [001] blocking the main channels as originally suggested by Meier (1961). The diffuse streaks restricted to $l = 2n + 1$ together with anomalies reported in powder diffractograms were interpreted as being either due to $\mathbf{c}$-axis faulting, intergrowth of different crystal varieties (Rudolf and Garcés 1994), or as a *c*/2 displacement of linear chains parallel to the main [001] channels (Campbell and Cheetham 2002). Song (1999) investigated defects in a commercial mordenite sample with high-resolution electron microscopy (HREM) and found in addition to dislocations with a displacement vector of 1/2 [110] two- and three-dimensional defects. The most frequent planar faults are displaced by 1/4 [010] resembling dachiardite, thus the pore size along $\mathbf{c}$ at the intergrowth boundary is reduced. Furthermore, blocks of dachiardite could be identified intergrown with the mordenite matrix.

This study presents (1) the successful synthesis of mordenite single-crystals with sufficient quality for single-crystal diffraction and (2) single-crystal diffraction data of both synthetic and natural mordenite to investigate the defect structure.

EXPERIMENTAL METHODS

Samples

For structural analysis a fibrous natural and a platy synthetic zeolite sample were used. The natural, K-rich mordenite single-crystal from Jarbridge, Nevada (Museum of Natural History Bern, NMBE-A9472), originating from jasper-covered vesicles of a strongly altered volcanic rock, was chemically analyzed by electron microprobe yielding the composition $K_{2.99}Ca_{1.85}Na_{1.06}Si_{40.15}Al_{7.89}O_{96}\cdot nH_2O$.

Pure mordenite-Na crystals were synthesized hydrothermally using a modified version of the method of Warzywoda et al. (1995). As discussed by Warzywoda et al. (1995, 1996) the mordenite crystal-size strongly depends on the surface area and porosity of the amorphous silica gel applied as the SiO_2 source in the hydrothermal experiments. The properties of silica gel are altered by subsequent heat treatment at elevated temperature (Warzywoda et al. 1995, 1996). After a series of test runs under various conditions we decided to add a small amount of ethanol (e.g., Sano

TABLE 1. Synthesis conditions for mordenite single-crystals

Batch Composition
$4.32Na_2O$, $19SiO_2$, $1Al_2O_3$, $293.6H_2O$
Source Materials
distilled water
sodium hydroxide (Hänseler)
sodium aluminate (Riedel-de Haen, anhydrous, technical)
silica gel (Aldrich, grade 62, 60–200 mesh, 150 Å; preheated 24 h at 850 °C under air)
ethanol
Batch preparation
(1) [0.1858 g sodium hydroxide + 1.8277 g distilled water], stir until dissolved
(2) [0.1147 g sodium aluminate and 1.8277g distilled water], stir until dissolved
(3) [(1) + (2) + 0.7989 g preheated silica gel + 2 ml ethanol], mix and stir for 30 min.
Crystallization
Teflon autoclave, 50 ml
Temperature: 175 °C
Time: 120 h
Product recovery
(1) Filter and wash
(2) Dry at 100 °C
References
Warzywoda et al. (1995, 1996)

TABLE 2. Experimental parameters for X-ray data collection and refinement of natural and synthetic mordenite

Sample	Natural mordenite	Synthetic mordenite
Crystal size (mm)	$0.05 \times 0.05 \times 0.30$	$0.06 \times 0.04 \times 0.05$
Diffractometer	Enraf-Nonius CAD4	Mar image plate
X-ray radiation	Mo$K\alpha$	Synchrotron (0.70192 Å)
Temperature	293 K	293 K
Space Group	$Cmc2_1$	$Cmc2_1$
Cell dimensions (Å)	18.096(4), 20.473(4), 7.515(2)	18.131(2), 20.507(2), 7.5221(5)
Absorption corr.	Empirical ψ-scans	none
Maximum 2θ	55.95	64.59
Measured reflections	3692	25625
Index range	$-10 \le h \le 23$, $-2 \le k \le 26$, $-1 \le l \le 9$	$-27 \le h \le 27$, $-30 \le k \le 30$, $-11 \le l \le 11$
Unique reflections	2099	5023
Reflections > 4σ(F_o)	1283	4930
R_{int}	0.0205	0.0483
R_σ	0.0398	0.0236
Number of l.s. parameters	178	163
GooF	0.975	1.206
$R1$, $F_o > 4\sigma(F_o)$	0.0335	0.0524
$R1$, all data	0.0855	0.0536
$wR2$ (on F_o^2)	0.0991	0.1360

et al. 2001) leading to an increase of the crystal size. The exact synthesis conditions are summarized in Table 1. The crystallization products were 100% mordenite with platy and uniform morphology. The run products were studied with a polarizing microscope and the single crystals were examined with a scanning electron-microscope and showed well-defined, but slightly curved faces and no apparent twinning. The average size of the mordenite crystals was about $0.07 \times 0.05 \times 0.05$ mm (Fig. 3). The chemical composition of the synthetic mordenite determined by electron microprobe was $Na_6Al_{6.02}Si_{42.02}O_{96}\cdot nH_2O$. The Si/Al ratio of 7/1 is in exact agreement with the analytical data given by Warzywoda et al. (1995) for their synthesis products obtained under corresponding conditions. According to Sand (1968) the applied synthesis conditions (175 °C and excess of sodium silicate) should lead to large-port mordenite. This property was tested by ion exchange with diluted solutions of bulky, organic dye molecules (Calzaferri et al. 2000) such as thionine blue ($C_{12}H_{10}N_3S^+$), methylene blue ($C_{16}H_{18}N_3S^+$), DAMS$^+$ ($C_{16}H_{19}N_2^+$), and benzothiazole dye ($C_{11}H_{14}NS^+$). Successful incorporation of dye ions could be monitored by polarized-light microscopy showing characteristic colors and pleochroism of the individual crystals (Simoncic and Armbruster 2002).
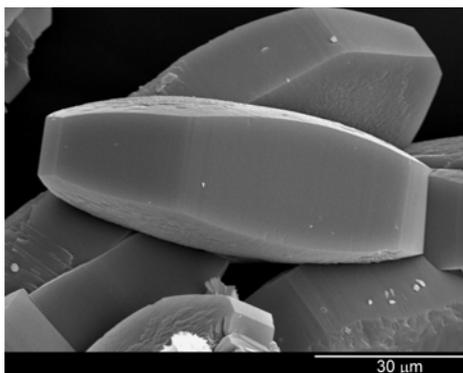
FIGURE 3. Scanning electron microscopic image of synthetic, platy mordenite of $Na_6Al_{6.02}Si_{42.02}O_{96}\cdot19H_2O$ composition. Notice that the (001) face is rough and slightly curved. The large channels (Figs. 1 and 2) run perpendicular to this face.

X-ray data collection

X-ray data collection of the fibrous natural mordenite ($0.05 \times 0.05 \times 0.30$ mm, elongated parallel to **c**) sample was performed at room temperature with an Enraf-Nonuis CAD4 single-crystal diffractometer using graphite monochromated Mo$K\alpha$ radiation. Additional experimental details are summarized in Table 2. Data reduction, including Lorentz and polarization correction, was performed with the SDP program package (Enraf-Nonius 1983).

X-ray data collection of the synthetic mordenite was performed at room temperature with synchrotron radiation (wavelength $\lambda = 0.70192$ Å) on the single crystal diffraction line at SNBL (ESRF, Grenoble) where diffracted intensities were registered with a MAR image plate. Data reduction was performed with the program package CrysAlis (Oxford Diffraction 2001). In the single crystal diffraction pattern of the synthetic mordenite sample, measured by synchrotron radiation, 76 reflections were observed which should be systematically absent, all with hkl values of $h + k = 2n$ and $l = 2n + 1$. Observation of these forbidden reflections is an artifact related to the frame-integration procedure and coincides with the diffuse scattering described below. Additional experimental details are given in Table 2.

Structure refinement

Structure refinement for both samples was carried out with the program SHELXL97 (Sheldrick 1997), using neutral-atom scattering factors (Si for all tetrahedral sites). Refinements were performed with anisotropic displacement parameters for all framework sites and highly populated extraframework positions. We have chosen a model with $Cmc2_1$ space-group symmetry. However, to reduce correlation effects due to pseudo-symmetry, we have constrained all framework atomic coordinates and displacement parameters to the counterpart related by an inversion operation (constrained sites are labeled with an additional prime symbol). Thus the tetrahedral framework is actually refined for $Cmcm$ symmetry, and $Cmc2_1$ symmetry accounts only for the extraframework part of the structure. The atom O8 linking the tetrahedra T2 and T2' with a T-O-T angle of 180° showed strong smearing perpendicular to the T-O bond. This O8 site was split into four closely spaced (ca. 0.5 Å) isotropic positions for which site-occupancy refinement yielded 25% occupancy each.

Difference Fourier analysis

After determining the common Si,Al framework and the extraframework cations and molecules, peaks remained in the difference Fourier maps (Figs. 4 and 5) of both the natural and synthetic sample. These peaks could not be assigned to extraframework occupants because distances to framework O atoms were too short. In addition, the coordinates of these peaks correspond almost exactly to the x,y-coordinates of the framework atoms but differ in the z-coordinate. Most obvious are the difference-Fourier peaks originating (Fig. 4) from the four-membered rings of tetrahedra shifted by $1/2\ c$ also reported by Mortier et al. (1975) for a dehydrated hydrogenated mordenite. If the residual peaks in the difference-Fourier map are analyzed in detail, counterparts of all framework positions can be found shifted by $1/2\ c$. Consequently the entire Si, Al framework is repeated but shifted by $c/2$. This unidirectional translation of the framework referred to as "domain B," may also be described by a (001) mirror plane at $z = 0$ and $z = 1/2$. Notice that in $Cmcm$
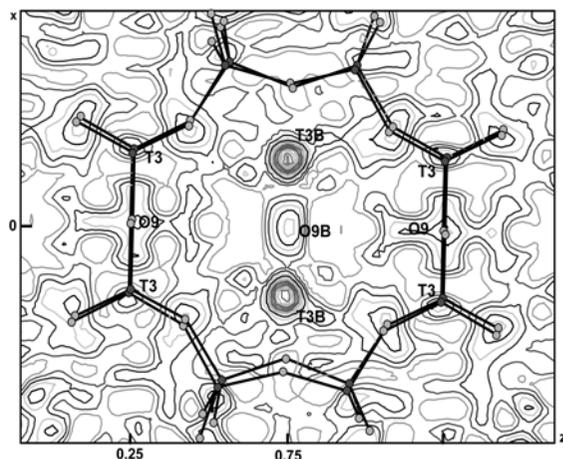

FIGURE 4. Difference-Fourier map of natural mordenite after introducing framework and extraframework positions. The (010) section at $y = 0.38$ shows a cross-section of the 8MRb channels. In addition, residual peaks (contours at 0.05 electrons intervals) in the center of the eight-membered ring indicate a replication of the T3-O9-T3 unit (edgewise view of the four-membered ring) but shifted by $1/2\ c$.
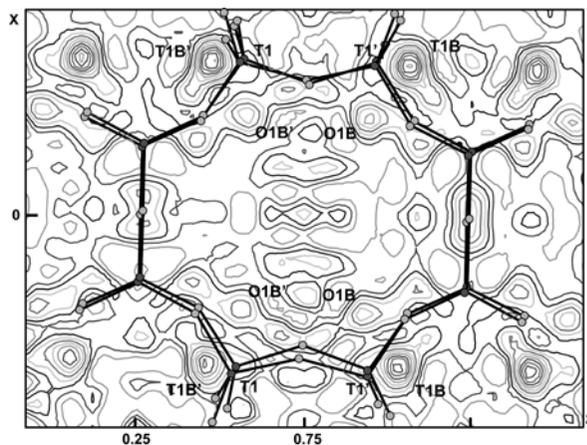

FIGURE 5. Difference-Fourier map of natural mordenite after introducing framework and extraframework positions. The (010) section at $y = 0.07$ shows a cross-section of the 8MRb channel. In addition, residual peaks (contours at 0.05 electrons interval) indicate a replication of the T1 site but shifted by $1/2\ c$. In addition, residual electron density of replicated O1B and O1B' (center at y = 0.09) can be seen. T1 and O1 are part of the puckered sheet of tetrahedra. This section shows that not only the four-membered ring pillars are shifted by $c/2$ (Fig. 4) but also the adjacent tetrahedral (100) sheets.

symmetry the (001) mirror plane is at $z = 1/4$ and $z = 3/4$. Figure 4 shows the (010) difference Fourier map section at $y = 0.38$ (which is close to the y-coordinate of the T3 and O9 framework atoms). The contoured peaks in the center of the rings correspond to the T3 and O9 atoms of the domain B. The z-coordinate of T3 and O9 is $1/4$ whereas z for T3B and O9B is $3/4$. Correspondingly, T4 and O10 of the B domain can be found in a (010) section with $y = 0.23$. To demonstrate that not only the four-membered ring pillars but the entire framework is reproduced by $c/2$ shifts, Figure 5 shows the (010) section of the difference Fourier map at $y = 0.07$, where the contoured peaks correspond to the T1B, T1B´, O1B, and O1B' atoms. T2B, T2B', O2B, and O2B' can correspondingly be found in a (010) section with $y = 0.31$.

In subsequent refinement cycles, the atomic coordinates of the $c/2$-shifted domain (B domain) were constrained to have identical x,y-coordinates as the major part of the structure and z of the so called B domain atoms was fixed at $z + 1/2$.
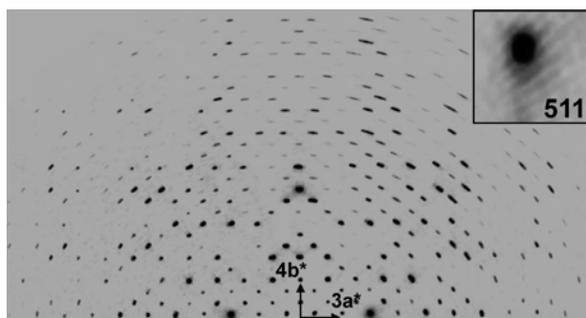
FIGURE 6. Reconstruction of the reciprocal $hk1$ layer from area detector measurements (synchrotron radiation) of a synthetic mordenite. Notice the diffuse halos particularly around the 511 and 0.12.1 reflections. The rod at $k = 0$ is extinct due to the c-glide in (010). However, the diffuse halos around 511 are smeared toward this empty rod. The slight radial streaking of the diffuse intensity is an artifact due to the reconstruction of the layer.
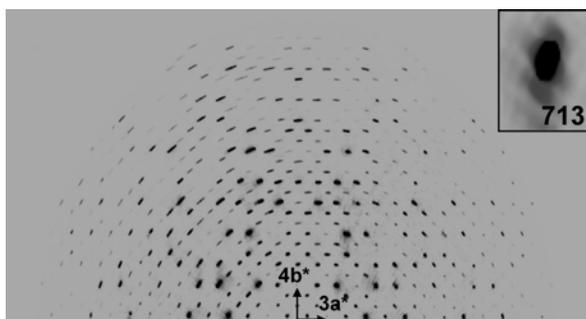
FIGURE 7. Reconstruction of the reciprocal $hk3$ layer from area detector measurements (synchrotron radiation) of a synthetic mordenite. Notice the diffuse halos, particularly around the following reflections: 713, 11.13, 443, 843, 10.43, 593, and 2.12.3. As in Figure 6, the rod at $k = 0$ is systematically extinct. However, the diffuse halos of reflections 713 and 11.13 are smeared toward this empty rod. The slight radial streaking of the diffuse intensity is an artifact due to the reconstruction of the layer.

The only exception is O8 (split into O8a, O8b, O8c, and O8d), which is common to both structural parts. Finally, a common population factor for all framework atoms of the A and B domain, respectively, was refined constraining A + B = 1. This refinement approach is consistent with the "fault plane model" used by Rudolf and Garcés (1994) in Rietveld refinements of synthetic mordenites. Introduction of the B domain in the refinement model of the nautral mordenite lowers R1 by ca. 0.5% and wR2 by ca. 1%.

RESULTS

Diffuse scattering

The X-ray single-crystal diffraction pattern from the synchrotron data show sharp Bragg reflections, but there are also diffuse intensities modulating the background of selected sharp peaks. To visualize the diffuse scattering, reciprocal space reconstructions of $hk0$, $hk1$, $hk3$, $h0l$, $h1l$, $h2l$, $0kl$, $1kl$, and $2kl$ layers were calculated using the CrysAlis software package (Oxford Diffraction 2001). Generally speaking, diffuse scattering is absent in all reciprocal layers with $l = 2n$, e.g., in $hk0$ and $hk2$. Diffuse scattering is also absent in the $h2l$ layer. Layers of the type hkl with $l = 2n + 1$ are diffuse where the diffuseness is not homogeneous but particularly concentrated around selected hkl reflections with
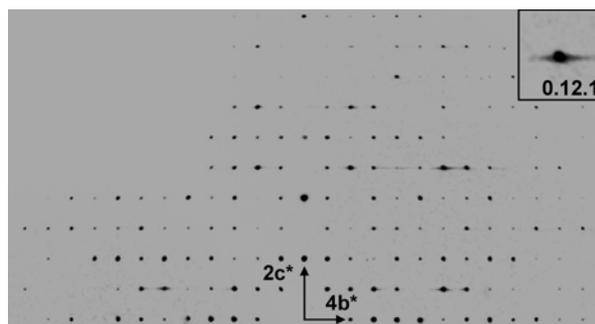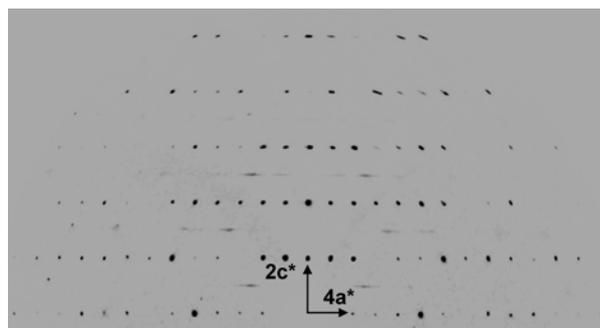

FIGURE 8. Reconstruction of the reciprocal $0kl$ layer from area detector measurements (synchrotron radiation) of a synthetic mordenite. Notice the streaking along $\mathbf{b}$* of the rods with $l = 2n + 1$.

FIGURE 9. Reconstruction of the reciprocal $h0l$ layer from area detector measurements (synchrotron radiation) of a synthetic mordenite. Notice the streaked intensities at 501, 703, 11.03, 505, etc. Corresponding intensities have been observed before in electron-diffraction studies and were interpreted as evidence for domains of I-centered symmetry (e.g., Sherman and Bennett 1973). These fake reflections are artifacts caused by the diffuse smearing of reflections in $\mathbf{b}$* adjacent layers as shown in Figs. 6 and 7.

$h + k = 2n$ (allowed by C-centering) as exemplified in the layers $hk1$ and $hk3$ (Figs. 6 and 7). Scattering (reflection smearing) is most accentuated around the reflections 511 and 0.12.1 in $hk1$, and 713, 11.13, 443, 843, 10.43, 593, and 2.12.3 in $hk3$. If the diffuse sheets with $l = 2n + 1$ are viewed in $0kl$, $1kl$, and $2kl$ reciprocal layers (Fig. 8) the diffuse sheets appear as diffuse streaks parallel to $\mathbf{b}$* decorated by sharp Bragg reflections. If the diffuse sheets with $l = 2n + 1$ are viewed, e.g., in $h0l$ reciprocal layers (Fig. 9) the diffuse sheets appear as diffuse maxima smeared along $\mathbf{a}$* at $h = 2n + 1$ and $l = 2n + 1$. Note that no reflections should occur in $h0l$ layers at $l = 2n + 1$ because of the c-glide in (010) for space group $Cmcm$ or $Cmc2_1$. The observed smeared maxima are diffuse residuals of the halos around the reflections in adjacent $h1l$ layers (e.g., reflections 511, 713). In other words, diffuse streaks or maxima in $0kl$ or $h0l$ layers are just traces of the diffuse hkl layers with $l = 2n + 1$.

Bragg reflections

The results of the structure refinement, comprising atomic coordinates, populations, and isotropic displacement parameters are given in Tables 3 and 4 for the natural and synthetic mordenite samples, respectively. Anisotropic displacement parameters are

TABLE 3. Atomic coordinates and B_{eq} (Å^2) values for natural mordenite from Jarbridge, Nevada

Atom	Population	x	y	z	B_{eq} (Å)
T1	0.973(2)	0.30126(4)	0.07249(4)	0.0419(1)	1.18(1)
T1'	0.973(2)	–0.30126(4)	–0.07249(4)	–0.0419(1)	1.18(1)
T2	0.973(2)	0.30343(4)	0.30905(4)	0.0457(1)	1.32(1)
T2'	0.973(2)	–0.30343(4)	–0.30905(4)	–0.0457(1)	1.32(1)
T3	0.973(2)	0.08719(6)	0.38323(5)	1/4	1.07(2)
T4	0.973(2)	0.08636(6)	0.22720(5)	1/4	1.14(2)
O1	0.973(2)	0.1239(1)	0.4161(1)	0.4290(3)	2.83(5)
O1'	0.973(2)	–0.1239(1)	–0.4161(1)	–0.4290(3)	2.83(5)
O2	0.973(2)	0.1228(1)	0.1941(1)	0.4268(3)	2.91(4)
O2'	0.973(2)	–0.1228(1)	–0.1941(1)	–0.4268(3)	2.91(4)
O3	0.973(2)	0.2372(2)	0.1227(1)	0.9858(4)	3.54(5)
O3'	0.973(2)	–0.2372(2)	–0.1227(1)	–0.9858(4)	3.54(5)
O4	0.973(2)	0.0976(2)	0.3048(2)	0.232(3)	2.7(1)
O5	0.973(2)	0.1698(2)	0.1949(2)	3/4	3.33(8)
O6	0.973(2)	0.1777(2)	0.4203(2)	3/4	2.65(6)
O7	0.973(2)	0.2686(2)	0	0	2.42(6)
O8a	0.25	0.2401(8)	0.2597(4)	0.529(4)	1.7(1)*
O8b	0.25	–0.2401(8)	–0.2597(4)	–0.529(4)	1.7(1)*
O8b	0.25	0.245(1)	0.251(1)	0.475(4)	1.7(1)*
O8d	0.25	–0.245(1)	–0.251(1)	–0.475(4)	1.7(1)*
O9	0.973(2)	0	0.4058(2)	1/4	2.13(8)
O10	0.973(2)	0	0.2054(2)	1/4	2.50(9)
Ca (8MRc)	0.466(8)	0	1/2	1/2	4.89(9)
K1a (12MRc)	0.24(2)	0	–0.0221(4)	0.267(4)	3.4(3)*
K1b (12MRc)	0.10(2)	0	–0.021(1)	0.166(4)	2.4(7)*
Na2a (12MRc)	0.47(1)	0	0.152(1)	0.691(3)	7.9(7)*
K2b (12MRc)	0.11(2)	0	0.130(2)	0.536(6)	6.5(14)*
K3 (12MRc)	0.24(2)	0	0.188(1)	0.782(3)	6.7(6)*
W1 (8MRb)	1.0	0	0.4315(4)	0.751(4)	6.9(2)
W2 (12MRc)	0.08(4)	0.369(4)	0.492(6)	3/4	4.9(31)*
W3 (12MRc)	0.53(4)	0.3734(9)	0.529(1)	0.715(3)	6.9(7)*
W4 (12MRc)	0.80(7)	0	0.071(1)	0.064(4)	10.26(5)*
W5 (12MRc)	0.23(4)	0.091(3)	0.060(3)	–0.168(7)	9.18(4)*
W6 (8MRb)	0.52(5)	0.033(1)	0.302(3)	0.694(5)	18.2(15)*
W7 (12MRc)	0.5	0.042(2)	0.065(1)	0.465(4)	11.1(8)*
W8 (12MRc)	0.42(8)	0	0.093(3)	–0.08(1)	11.3(23)*
W9 (12MRc)	0.30(5)	–0.105(2)	0.021(3)	–0.064(8)	11.4(24)*
W10 (12MRc)	0.32(4)	0.403(3)	0.453(3)	0.82(1)	19.1(33)*
T1B	0.027(2)	0.30126(4)	0.07249(4)	–0.0419(1)	2.37*
T1B'	0.027(2)	–0.30126(4)	–0.07249(4)	0.0419(1)	2.37*
T2B	0.027(2)	–0.30343(4)	–0.30905(4)	0.0457(1)	2.37*
T2B'	0.027(2)	0.30343(4)	0.30905(4)	–0.0457(1)	2.37*
T3B	0.027(2)	0.08719(6)	0.38323(5)	3/4	2.37*
T4B	0.027(2)	0.08636(6)	0.22720(5)	3/4	2.37*
O1B	0.027(2)	0.1239(1)	0.4161(1)	–0.4290(3)	2.37*
O1B'	0.027(2)	–0.1239(1)	–0.4161(1)	0.4290(3)	2.37*
O2B	0.027(2)	0.1228(1)	0.1941(1)	–0.4268(3)	2.37*
O2B'	0.027(2)	–0.1228(1)	–0.1941(1)	0.4268(3)	2.37*
O3B	0.027(2)	0.2372(2)	0.1227(1)	–0.9858(4)	2.37*
O3B'	0.027(2)	–0.2372(2)	–0.1227(1)	0.9858(4)	2.37*
O4B	0.027(2)	0.0976(2)	0.3048(2)	–0.232(3)	2.37*
O5B	0.027(2)	0.1698(2)	0.1949(2)	1/4	2.37*
O6B	0.027(2)	0.1777(2)	0.4203(2)	1/4	2.37*
O7B	0.027(2)	0.2686(2)	0	1/2	2.37*
O9B	0.027(2)	0	0.4058(2)	3/4	2.37*
O10B	0.027(2)	0	0.2054(2)	3/4	2.37*

Notes: Refinement in space group $Cmc2_1$ with all framework positions constrained to $Cmcm$ symmetry. All atomic positions labeled B are fully constrained and belong to a domain of mordenite shifted $c/2$ relative to the main part of the structure.

* Starred atoms with standard deviation were refined isotropically, those without standard deviations were fixed. Anisotropically refined atoms are given in the form of the isotropic equivalent thermal parameter defined as $B_{eq} = 8/3\ \pi^2 \sum_i(\sum_j(U_{ij}\ a_i^*\ a_j^*\ a_i.a_j))$

TABLE 4. Atomic coordinates and B_{eq} (Å^2) values for synthetic mordenite-Na

Atom	Population	x	y	z	B_{eq} (Å)
T1	0.968(1)	0.30243(2)	0.07270(2)	0.04241(5)	1.106(6)
T1'	0.968(1)	–0.30243(2)	–0.07270(2)	–0.04241(5)	1.106(6)
T2	0.968(1)	0.30335(2)	0.30941(2)	0.04531(5)	1.158(6)
T2'	0.968(1)	–0.30335(2)	–0.30941(2)	–0.04531(5)	1.158(6)
T3	0.968(1)	0.08689(3)	0.38261(2)	1/4	0.955(7)
T4	0.968(1)	0.08638(3)	0.22709(2)	1/4	0.990(7)
O1	0.968(1)	0.12280(8)	0.41515(8)	0.4284(2)	2.82(2)
O1'	0.968(1)	–0.12280(8)	–0.41515(8)	–0.4284(2)	2.82(2)
O2	0.968(1)	0.12248(8)	0.19422(7)	0.4266(2)	2.54(2)
O2'	0.968(1)	–0.12248(8)	–0.19422(7)	–0.4266(2)	2.54(2)
O3	0.968(1)	–0.23715(9)	–0.12207(7)	–0.9887(2)	3.44(3)
O3'	0.968(1)	0.23715(9)	0.12207(7)	0.9887(2)	3.44(3)
O4	0.968(1)	0.0983(1)	0.30462(9)	0.248(1)	3.29(5)
O5	0.968(1)	0.1700(1)	0.1937(1)	3/4	3.17(4)
O6	0.968(1)	0.1750(1)	0.4205(1)	3/4	2.46(3)
O7	0.968(1)	0.2708(1)	0	0	2.39(3)
O8a	0.25	0.2401(6)	0.2602(4)	0.532(1)	1.66(6)*
O8b	0.25	–0.2401(6)	–0.2602(4)	–0.532(1)	1.66(6)*
O8c	0.25	0.2446(5)	0.2521(5)	0.480(1)	1.66(6)*
O8d	0.25	–0.2446(5)	–0.2521(5)	–0.480(1)	1.66(6)*
O9	0.968(1)	0	0.4034(1)	1/4	2.24(4)
O10	0.968(1)	0	0.2069(1)	1/4	2.24(4)
Na1 (8MRc)	0.290(5)	0.0118(2)	–0.5073(2)	0.5104(8)	2.3(1)*
Na2 (12MRc)	0.09(1)	0	0.008(1)	–0.229(4)	3.3(6)*
Na3 (12MRc)	0.26(2)	0	0.201(2)	0.774(6)	9.87*
Na4a (12MRc)	0.21(2)	0	0.072(2)	0.495(8)	9.87*
Na4b (12MRc)	0.23(2)	0	0.080(2)	0.019(7)	9.87*
W1 (8MRb)	1.0	0	0.4344(3)	0.754(2)	6.2(1)
W2 (12MRc)	0.31(1)	0.128(1)	–0.0151(9)	0.222(3)	7.90*
W3 (12MRc)	0.40(3)	1/2	0.332(2)	0.269(5)	7.90*
W4 (12MRc)	0.22(1)	0.111(1)	–0.019(1)	0.018(5)	7.90*
W5 (12MRc)	0.27(1)	0.103(1)	–0.040(1)	0.354(3)	7.90*
W6 (12MRc)	0.32(1)	1/2	0.223(1)	0.302(4)	7.90*
W7 (12MRc)	0.22(1)	1/2	0.383(2)	0.379(7)	7.90*
W8 (8MRb)	0.24(1)	0.455(1)	0.190(1)	0.195(3)	7.90*
W9 (12MRc)	0.20(2)	1/2	0.321(3)	0.128(8)	7.90*
W10 (12MRc)	0.18(2)	1/2	0.447(2)	–0.205(7)	7.90*
W11 (12MRc)	0.46(3)	1/2	0.388(1)	0.017(4)	7.90*
T1B	0.032(1)	0.30243(2)	0.07270(2)	–0.04241(5)	2.37*
T1B'	0.032(1)	–0.30243(2)	–0.07270(2)	0.04241(5)	2.37*
T2B	0.032(1)	–0.30335(2)	–0.30941(2)	0.04531(5)	2.37*
T2B'	0.032(1)	0.30335(2)	0.30941(2)	–0.04531(5)	2.37*
T3B	0.032(1)	0.08689(3)	0.38261(2)	3/4	2.37*
T4B	0.032(1)	0.08638(3)	0.22709(2)	3/4	2.37*
O1B	0.032(1)	0.12280(8)	0.41515(8)	–0.4284(2)	2.37*
O1B'	0.032(1)	–0.12280(8)	–0.41515(8)	0.4284(2)	2.37*
O2B	0.032(1)	0.12248(8)	0.19422(7)	–0.4266(2)	2.37*
O2B'	0.032(1)	–0.12248(8)	–0.19422(7)	0.4266(2)	2.37*
O3B	0.032(1)	–0.23715(9)	–0.12207(7)	0.9887(2)	2.37*
O3B'	0.032(1)	0.23715(9)	0.12207(7)	–0.9887(2)	2.37*
O4B	0.032(1)	0.0983(1)	0.30462(9)	–0.248(1)	2.37*
O5B	0.032(1)	0.1700(1)	0.1937(1)	1/4	2.37*
O6B	0.032(1)	0.1750(1)	0.4205(1)	1/4	2.37*
O7B	0.032(1)	0.2708(1)	0	1/2	2.37*
O9B	0.032(1)	0	0.4034(1)	3/4	2.37*
O10B	0.032(1)	0	0.2069(1)	3/4	2.37*

Notes: Refinement in space group $Cmc2_1$ with all framework positions constrained to $Cmcm$ symmetry. All atomic positions labeled B are fully constrained and belong to a domain of mordenite shifted $c/2$ relative to the main part of the structure.

* Starred atoms with standard deviation were refined isotropically, those without standard deviations were fixed. Anisotropically refined atoms are given in the form of the isotropic equivalent thermal parameter defined as $B_{eq} = 8/3\ \pi^2 \sum_i(\sum_j(U_{ij}\ a_i^*\ a_j^*\ a_i.a_j))$

in Tables 5 and 6; Tables 7 and 8 summarize T-O distances and T-O-T angles of the tetrahedral framework.

DISCUSSION

Si, Al arrangement

Distortions within the tetrahedral framework structure are very similar for synthetic and natural mordenite as estimated from T-O-T angles (Tables 7 and 8). Major differences in T-O-T angles occur only for angles within the four-membered rings. These angles are ca. 2° larger in the synthetic sample than in the natural one. Removing O8 from the inversion center and splitting it into four 25% occupied sites reduced the T2-O8-T2' angle from 180° to 155–167°.

Judging from the average <T-O> bond length there is also

TABLE 5. Anisotropic displacement parameters U_{ij} of natural mordenite from Jarbridge, Nevada

Atom	U_{11}	U_{22}	U_{33}	U_{12}	U_{13}	U_{23}
T1	0.0192(4)	0.0154(3)	0.0103(3)	0.0018(3)	0.0018(3)	0.0008(3)
T1′	0.0192(4)	0.0154(3)	0.0103(3)	0.0018(3)	0.0018(3)	0.0008(3)
T2	0.0208(4)	0.0172(3)	0.0121(4)	0.0037(4)	0.0012(3)	–0.0013(3)
T2′	0.0208(4)	0.0172(3)	0.0121(4)	0.0037(4)	0.0012(3)	–0.0013(3)
T3	0.0117(5)	0.0158(5)	0.0132(5)	–0.0017(4)	0	0
T4	0.0119(5)	0.0162(5)	0.0153(5)	0.0013(4)	0	0
O1	0.030(1)	0.055(2)	0.023(1)	–0.007(1)	–0.008(1)	–0.006(1)
O1′	0.030(1)	0.055(2)	0.023(1)	–0.007(1)	–0.008(1)	–0.006(1)
O2	0.032(1)	0.051(1)	0.028(1)	0.000(1)	–0.009(1)	0.010(1)
O2′	0.032(1)	0.051(1)	0.028(1)	0.000(1)	–0.009(1)	0.010(1)
O3	0.052(2)	0.035(1)	0.047(2)	0.021(1)	–0.006(1)	0.005(1)
O3′	0.052(2)	0.035(1)	0.047(2)	0.021(1)	–0.006(1)	0.005(1)
O4	0.036(2)	0.019(1)	0.048(7)	–0.002(2)	0.011(4)	0.001(4)
O5	0.052(2)	0.057(2)	0.016(2)	0.017(2)	–0.020(6)	0.008(8)
O6	0.045(2)	0.042(2)	0.013(1)	–0.008(2)	0	0
O7	0.033(2)	0.021(1)	0.038(2)	0	0	–0.005(1)
O9	0.015(2)	0.030(2)	0.036(3)	0	0	–0.01(1)
O10	0.019(2)	0.029(3)	0.047(3)	0	0	0
Ca	0.056(3)	0.065(3)	0.065(3)	0	0	–0.037(2)
W1	0.050(4)	0.080(5)	0.133(9)	0	0	–0.05(1)

TABLE 6. Anisotropic displacement parameters U_{ij} of synthetic mordenite–Na

Atom	U_{11}	U_{22}	U_{33}	U_{12}	U_{13}	U_{23}
T1	0.0187(2)	0.0126(2)	0.0107(2)	0.0017(1)	0.0017(1)	0.0013(1)
T1′	0.0187(2)	0.0126(2)	0.0107(2)	0.0017(1)	0.0017(1)	0.0013(1)
T2	0.0174(2)	0.0149(2)	0.0117(2)	0.0033(1)	0.0007(1)	–0.0011(1)
T2′	0.0174(2)	0.0149(2)	0.0117(2)	0.0033(1)	0.0007(1)	–0.0011(1)
T3	0.0108(2)	0.0132(2)	0.0123(2)	–0.0016(2)	0	0
T4	0.0102(2)	0.0130(2)	0.0145(2)	0.0012(2)	0	0
O1	0.0305(6)	0.0523(8)	0.0242(5)	–0.0086(6)	–0.0094(5)	–0.0072(5)
O1′	0.0305(6)	0.0523(8)	0.0242(5)	–0.0086(6)	–0.0094(5)	–0.0072(5)
O2	0.0282(6)	0.0432(8)	0.0252(6)	–0.0023(5)	–0.0093(5)	0.0087(5)
O2′	0.0282(6)	0.0432(8)	0.0252(6)	–0.0023(5)	–0.0093(5)	0.0087(5)
O3	0.0502(9)	0.0332(7)	0.0472(8)	0.0229(6)	–0.0072(7)	0.0063(6)
O3′	0.0502(9)	0.0332(7)	0.0472(8)	0.0229(6)	–0.0072(7)	0.0063(6)
O4	0.035(1)	0.0146(8)	0.076(2)	0.0030(7)	0.021(3)	0.017(2)
O5	0.044(1)	0.061(2)	0.0150(8)	0.019(1)	–0.016(2)	–0.017(2)
O6	0.040(1)	0.041(1)	0.0118(6)	–0.0071(8)	0	0
O7	0.0333(9)	0.0193(7)	0.0382(9)	0	0	–0.0061(7)
O9	0.0149(9)	0.033(1)	0.038(1)	0	0	0.019(3)
O10	0.0127(9)	0.031(1)	0.042(1)	0	0	0
W1	0.062(3)	0.097(4)	0.078(4)	0	0	–0.042(6)

TABLE 7. T-O distances (Å) and T-O-T angles (°) of natural mordenite

Bond		Al%	Bond		Al%
T1-O1	1.616(2) [1.634]		T2-O2	1.608(2) [1.625]	
T1-O3′	1.605(3) [1.631]		T2-O5	1.612(1) [1.630]	
T1-O6	1.616(1) [1.633]		T2-O8ave	1.61(1)	
T1-O7	1.628(1) [1.641]		T2-O3	1.597(2) [1.622]	
average	1.616 [1.635]	7.9	average	1.606 [1.621]	1.5
		Norm. 14			Norm. 3
T3-O1	1.644(2) [1.663]		T4-O2	1.631(2) [1.650]	
T3-O4	1.622(4) [1.640]		T4-O4	1.608(4) [1.626]	
T3-O9	1.644(2) [1.655]		T4-O10	1.625(2) [1.639]	
T3-O1′	1.644(2) [1.663]		T4-O2′	1.631(2) [1.650]	
average	1.639 [1.656]	22.7	average	1.624 [1.641]	13.0
		Norm. 41			Norm. 24
T1-O1-T3	145.83(18)		T2-O2-T4	143.58(17)	
T1′-O3-T2	158.1(2)		T3-O4-T4	163.0(8)	
T2-O5-T2′	144.5(3)		T1-O6-T1′	150.8(3)	
T1-O7-T1′	137.4(2)		T2-O8A/C-T2′	155(1) / 165(1)	
T3-O9-T3	147.4(3)		T4-O10-T4	148.2(3)	

Notes: Uncorrected T-O distances with standard deviations in parentheses and T-O distances corrected for riding motion (Johnson 1970) in brackets. Al% is estimated from the relationship by Jones (1968). Norm. refers to the Al% (Jones 1968) normalized to the analyzed Al bulk composition.

TABLE 8. T-O distances (Å) and T-O-T angles (°) of synthetic mordenite-Na

Bond		Al%	Bond		Al%
T1-O1	1.6232(13) [1.642]		T2-O2	1.6160(14) [1.631]	
T1-O3′	1.6092(14) [1.636]		T2-O5	1.6148(8) [1.635]	
T1-O6	1.6203(6) [1.636]		T2-O8ave.	1.6184(6)	
T1-O7	1.6291(8) [1.643]		T2-O3	1.6060(13) [1.632]	
average	1.620 [1.639]	10.5	average	1.614 [1.629]	6.6
		Norm. 13			Norm. 8
T3-O1	1.6343(13) [1.655]		T4-O2	1.6269(13) [1.644]	
T3-O4	1.6124(19) [1.640]		T4-O4	1.6047(19) [1.631]	
T3-O9	1.6319(9) [1.646]		T4-O10	1.6202(9) [1.634]	
T3-O1′	1.6343(13) [1.655]		T4-O2′	1.6269(13) [1.644]	
average	1.628 [1.649]	15.6	average	1.620 [1.638]	10.5
		Norm. 20			Norm. 13
T1-O1-T3	146.01(11)		T2-O2-T4	143.61 (10)	
T1′-O3-T2	157.95(13)		T3-O4-T4	164.82(16)	
T2-O5-T2′	144.92(15)		T1-O6-T1′	149.04 (14)	
T1-O7-T1′	138.72(12)		T2-O8A/C-T2′	154.2(9) / 166.7(4)	
T3-O9-T3	149.74(18)		T4-O10-T4	150.33(19)	

Notes: Uncorrected T-O distances with standard deviations in parentheses and T-O distances corrected for riding motion (Johnson 1970) in brackets. Al% is estimated from the relationship by Jones (1968). Norm. refers to the Al% (Jones 1968) normalized to the analyzed Al bulk composition.

a significant difference in Si,Al order between natural and the synthetic mordenite. The <T1-O> and <T2-O> bond lengths of the synthetic crystal are slightly larger than for the natural one. On the other hand <T3-O> and <T4-O> bond lengths of the natural crystal are larger than for the synthetic one. T1 and T2 tetrahedra assemble the puckered (100) sheets whereas T3 and T4 tetrahedra belong to the four-membered rings connecting the sheets to a framework. It has been shown (Alberti et al. 1986; Alberti and Gottardi 1988) that the Jones (1968) relationship (Al = 6.4116 <T-O> -10.282) fails to predict reliable Al concentrations for mordenite. Actually, the Jones (1968) relationship yields 4.36 Al p.f.u. (measured 7.89 Al p.f.u.) for the natural crystal and 4.82 Al p.f.u. (measured 6.02 Al p.f.u.) for the synthetic one. We have also applied a riding correction (Johnson 1970) for T-O bond length (due to rigid librational disorder of TO_4 moieties). However, the T-O riding correction is very similar for both structures and can not explain the drastic Al underestimation for the natural crystal. If we normalize, as a rough estimate, the Al distribution from the Jones (1968) relationship to the analyzed Al concentration we obtain the following Al distribution pattern: T1 (nat: 0.14, syn: 0.13), T2 (nat: 0.03, syn: 0.08), T3 (nat: 0.41, syn: 0.20), and T4 (nat: 0.24, syn: 0.13). The values for the natural crystal

are actually very similar to the normalized average calculated by Alberti (1997) from literature data for natural or ion-exchanged natural mordenites. Unfortunately, the series of Rietveld powder refinements by Shiokawa et al. (1989) and Rudolf and Garcés (1994) on synthetic mordenites with Al between 3.55 and 7.87 p.f.u. does not, due to insufficient quality of the T-O bond lengths, allow us to draw any conclusions on Si,Al order. All natural mordenites (Passaglia 1975) have approximately 2 Ca p.f.u. as extraframework occupants. Ca occupies the center of the 8MRc ring (Alberti et al. 1986; Ito and Saito 1985; this study) and bonds to O1, O1', and O9 that are additionally bonded to T3, which is strongly Al enriched in natural samples. Thus we suggest a synergetic effect between extraframework occupants and Si,Al order during crystal growth. In synthetic mordenite, grown in a pure Na alkaline environment, there is less extraframework charge close to T3 and correspondingly less Al at T3 for local charge balance. Analogous interplay between extraframework cations and Si,Al order has been analyzed for heulandite (Akizuki et al.

1999) and was considered responsible for the different selectivity of alkali and alkaline earth cations in exchange experiments (Tarasevich et al. 2002).

Extraframework cations

The analytically determined extraframework-cation content of the natural mordenite sample was $K_{2.99}Ca_{1.85}Na_{1.06}$ whereas the composition $K_{2.77}Ca_{1.86}Na_{1.90}$ was obtained from the structure refinement. The excess of refined Na may be explained by some Na/H_2O disorder. Ca (population 0.47) is situated in the center of the strongly compressed eight-membered channel and has short distances to the framework O atoms O1, O1', O9 (2×2.87, 2×2.87, 2×2.69 Å) and bonds twice to H_2O molecule W1 (2.29, 2.35 Å) with an angle of 180°. If we further assume that the site assignment of Ca is correct (Ito and Saito 1985; Alberti et al. 1986) then ca. 4.8 positive charges p.f.u. remain in 12MRc and are easily accessible for cation exchange. K1 (1.36 p.f.u.) is split into K1a (population: 0.24) and K1b (population: 0.10), separated by 0.8 Å along **c**. These sites are not bonded to the tetrahedral framework but are surrounded by strongly disordered H_2O in 12MRc whereas K3 occupies pockets, which are defined as the transit from 12MRc to 8MRb. Na2a (population: 0.47) and K2b (population: 0.11) are separated by 1.2 Å along the **c** axis. Therefore, K2b appears to be a satellite position indicating translational disorder along the **c** axis. Na2a has no bonds to the tetrahedral framework whereas K2b bonds twice to O2 (2.71 Å) and once to O10 (2.65 Å). The K3 site was identified by the long distances to the framework with two bonds to O5 (3.09 Å) and one bond to O2' (3.12 Å).

The synthetic mordenite sample has 6 Na in the channel system, whereas 5.5 Na p.f.u. were located by the structure refinement. With 2.3 Na1 p.f.u. (population: 0.29) located in the strongly compressed 8MRc, ca. 3.7 positive charges are in 12MRc. In contrast to the Ca site in the natural sample the corresponding Na1 site in the synthetic material is shifted from the special position and has four short bonds to the tetrahedral framework (Na1-O1: 2.64, Na1-O9: 2.69 and 2.80, Na1-O1': 2.80 Å). Na2 and Na3 (2.2 p.f.u.) are not bonded to the tetrahedral framework but are surrounded by strongly disordered H_2O in 12MRc and only Na4a,b (1 p.f.u.) occupy the pocket at the transition to 8MRb but without short bonds to the framework.

Limitations of the Bragg model

Even after introducing the domain B, there are various weak peaks (<0.5 e/Å³) in the difference Fourier map from the synchrotron data of the synthetic crystal that could be interpreted as an indicator of a slightly different conformation within the puckered (100) sheet formed by six-membered rings. These peaks have either suspicious distances of 1.6 Å to existing T sites or they are approximately 1.6 Å from located O sites. Considering the high quality synchrotron data and the significant but very low contribution from diffuse scattering there are some nonsatisfying parameters in Table 2. The value R_{int}, estimating the agreement of symmetry equivalent reflections, is twice as high as R_σ from counting statistics. Even the $R1$ and $wR2$ values (agreement between structure model and observed structure factors) determined in the course of the structure refinement are rather high. We offer three explanations for the above insufficiencies: (1) the

diffraction data also contains information on the defect (100) layer (discussed below) which becomes necessary to link two identical structural blocks shifted by $c/2$. (2) Contributions from Bragg diffraction and diffuse scattering were not discriminated in the peak integration procedure. Thus the integrated intensity of Bragg reflections is significantly influenced by the diffuse-scattering contribution. This is especially important for weak or symmetry-forbidden reflections, which are influenced by the diffuse halos of adjacent reflections. And (3) the assumed *Cmcm* pseudosymmetry of the tetrahedral framework is only a fair approximation. This latter argument is supported by the microtwin model (Meier et al. 1978; Gramlich-Meier 1981).

Defects and crystallographic faults

First investigations of possible faults were discussed by Sherman and Bennett (1973) suggesting *Cmmm*, *Immm*, and *Imcm* intergrowth with *Cmcm* symmetry in the mordenite structure. Based on our diffuse scattering results and the electron diffraction pattern discussed by Sanders (1985) this intergrowth model must be viewed with skepticism because it is mainly based on space-group violating reflections in *h0l* reciprocal layers. As discussed above such diffuse reflections are artifacts and result from diffuse halos of adjacent layers. The probable misinterpretation of structural intergrowth (Sherman and Bennet 1973) is related to the lack of electron-diffraction patterns along [001] which were difficult to access at the time due to the fibrous character and the pronounced (100) cleavage of mordenite. Thus a correct interpretation of diffuse diffraction maxima in *h0l* layers was hampered.

There are highly confusing evidences in the literature concerning the importance of $c/2$ faults in synthetic mordenite. Better understanding of this subject becomes best evident in a short historic review. Mortier et al. (1975) studied a natural mordenite from Challis Valley, Idaho. After refining the tetrahedral framework structure Mortier et al. (1975) noticed in difference Fourier maps a repetition of four-ring pillar domains, ca. 2% (composed of T3B, T4B, O4B, O9B, O10B) shifted by $c/2$ relative to the four-ring pillars of the major *Cmcm* structure. The same type of defects (ca. 4%) were also observed for dehydrated and rehydrated K-exchanged mordenite from the same locality (Mortier et al. 1978). A series of very fine crystalline synthetic mordenites with varying Si/Al ratios between 5.1 and 9.5 was produced by Itabashi et al. (1986). X-ray powder diffractograms of these mordenites exhibited intensity ratios of the reflections 111/130 and 241/002 which increased linearly with Si/Al ratio. Thus these intensity ratios were considered characteristic of the Si/Al ratio in mordenite. In a subsequent Rietveld refinement by Shiokawa et al. (1989) of essentially the same samples, it was stated that there is no substantial change in the framework with Si/Al ratio and that the observed variation in powder intensity ratios can be explained by shifts and occupancies of the extraframework atoms. Rudolf and Garcés (1994) analyzed the theoretical influence of the $c/2$ shifted four-ring pillars on the X-ray powder pattern and restudied samples from the same source as Shiokawa et al. (1989) by Rietveld methods, which suggested that $c/2$ faults not only relate to the four-ring pillars, but also to complete structural domains of the *Cmcm* structure. They subsequently refined the large value of 21% of $c/2$ shifted

domains from powder data of synthetic sodium mordenite with Si/Al = 5.25. The striking dependence of the 111/130 reflection-intensity ratio in X-ray powder patterns with the Si/Al ratio in the mordenite framework was revived by Campbell and Cheetham (2002) analyzing the theoretical influence of $c/2$ shifts on this intensity ratios. Campbell and Cheetham (2002) determined that the odd-l reflection intensities are rapidly extinguished as the $c/2$ defect concentrations increase, while the even-l intensities are relatively unaffected. As conclusion they offer a semi-quantitative diagram for defect concentration vs. percentage of Al content in the framework. For our compositions (nat. = 16% Al, syn.= 12.5% Al) ca. 0.25 and ca. 0.15 defect portions would be predicted. This is almost one order of magnitude higher than the $c/2$ defect concentrations determined in this study (0.027 and 0.031, respectively). The physical argument (Campbell and Cheetham 2002) for the increase of defect concentration with Al content is: "During crystal formation, the longer Al-O bonds may cause a new pillar to bond more favorably at the $c/2$ shifted position. Once initiated, such a defect could propagate along [001] during subsequent crystal growth to avoid the disruptive pillar spacings associated with its termination."

A general relationship between Al-content and defect concentration as might be derived from the arguments by Campbell and Cheetham (2002) and Rudolf and Garcés (1994) cannot be confirmed by our data. Well-crystallized synthetic mordenites do not follow this trend. In contrast, they show similar defect concentrations as found for well-crystallized natural mordenites. It seems that crystal-growth conditions are more decisive than just the Al concentration in the framework.

Furthermore, the fact that in structure refinements of natural mordenites (with ca. 15–20% Al) either only very weak indications of B type domains were detected or these domains could not be resolved suggests that in none of these studies B type domains exceeded concentration levels above ca. 5%. This is an additional argument against a general relationship between Al concentration and amount of B type domains.

Structural model for defect layer

The occurrence of two domains, which exist side by side in the mordenite structure, makes it necessary to find a structural conformation for a coherent connection of such domains. As already stated by Meier (1978) four-ring pillars cannot be shifted along **c** without reconstruction of the puckered (100) sheets. A possible linkage is presented which is consistent with the model of Campbell and Cheetham (2002). This model is strictly empirical and not derived from "ghost" peaks in difference-Fourier maps or from diffuse scattering contributions.

The puckered (100) sheets of faultless mordenite consist of six-membered rings where half of the tetrahedral apices point upward and half point downward. This tetrahedral conformation allows the construction of a three-dimensional zeolite framework by bonding the four-membered rings to the (100) sheets (Fig. 10). Domain B is now introduced by shifting the overlying four-membered rings by $c/2$. However, to enable strain-free linkage of the shifted pillars, the puckered (100) sheet has to be reconstructed. The relevant tetrahedra are tilted so that the upward-pointing apices form a new connection and two new apices are free for bonding to the four-member rings of domain B
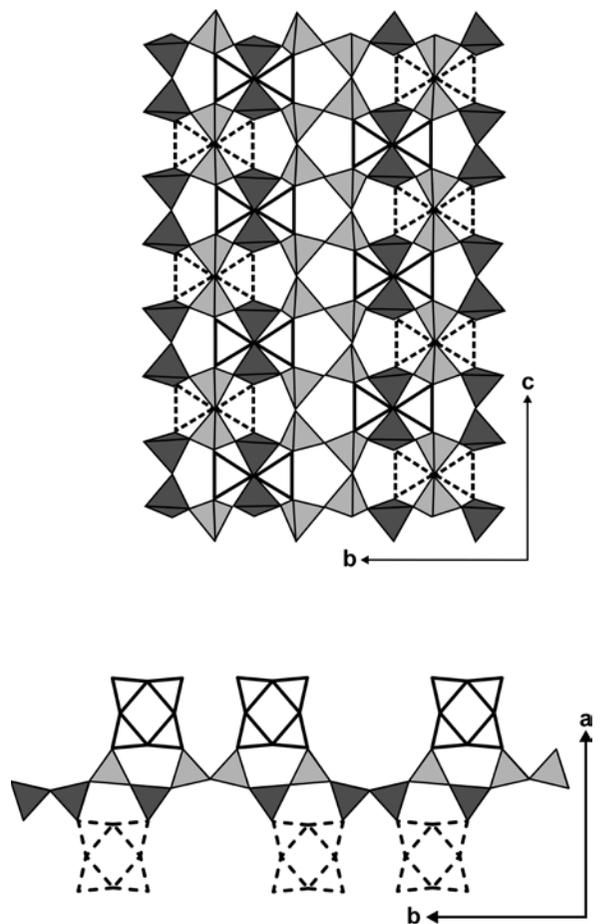

FIGURE 10. (**a**) The puckered (100) sheet formed by six-membered rings of tetrahedra in faultless mordenite is viewed down **a**. Light grey tetrahedra point upward, dark grey tetrahedra point downward. Triangles with full lines represent overlying four-membered rings (seen edge-wise), dotted lines the underlying ones. (**b**). The same (100) sheet with adjacent four-membered rings projected down **c**. Downward-pointing tetrahedra bond to underlying rings (at $z = 0$); upward-pointing tetrahedra bond to overlying rings (at $z = 1/2$).
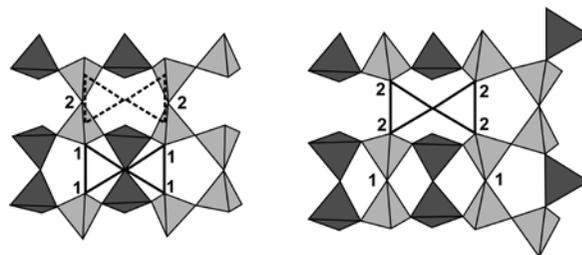

FIGURE 11. Detailed view of the (100) sheet (compare with Fig.10). Left: Triangles with solid outlines show the position of the overlying unshifted four-member rings. Dotted lines represent the $c/2$ shifted positions of four-membered rings belonging to domain B. Numbers (1, 2) indicate tetrahedral apices which need to be rearranged to allow bonding to the $c/2$ shifted four-membered ring pillars. Right: Breaking of bonds between upward pointing apices and a four-membered ring (1) and disrupting a connection of two adjacent upward pointing apices (2). New linkage of the two apices labeled (1) and new bonding of the apices labeled (2) to the four-membered rings of the overlying domain B.
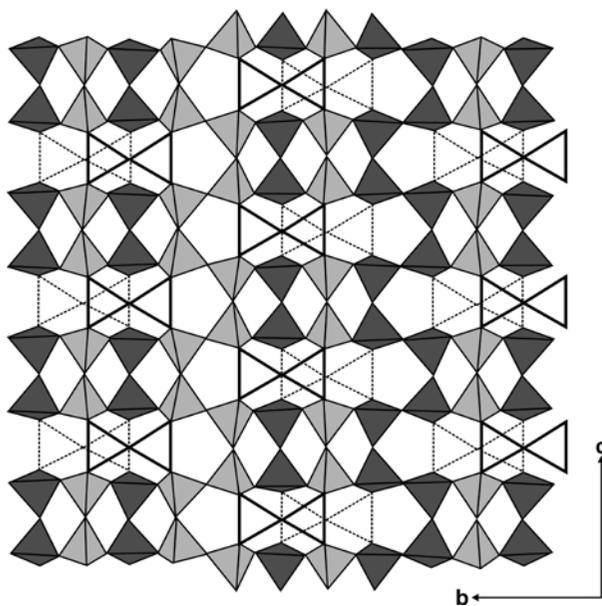
FIGURE 12. (100) defect layer projected down **a**. Light gray tetrahedra are pointing upward, dark gray ones point downward. Solid lines mark the position of the four-membered rings (seen edge-wise) belonging to the overlying domain B. Fine dotted lines show the underlying four-membered rings of domain A. Three four-membered rings are flanked by compressed 12-membered rings forming rows along **b**.

(Fig. 11). The new defect layer linking domain A and B consists of three edge-sharing four-member rings flanked by a strongly compressed 12-membered ring forming rows along **b** (Fig. 12). The defect layer does not affect the large 12MRc tubes. This is of great importance because these channels provide the catalytic properties of mordenite.

Diffuse scattering

Our observations of diffuse scattering correspond very well with the electron diffraction results of Sherman and Bennett (1973) and Sanders (1985). Even if we were not able to measure (point detector) the diffuse scattering for the natural crystal, it is clear that this is a common feature also for the natural mordenite investigated. The scattering in synthetic mordenite is also concentrated around points with $h + k = 2n$ and appears only if $l = 2n + 1$. Instead of continuous streaks in the $h0l$ section or odd and even maxima, we only observed streaks with distinct maxima at odd h values. These intensities may not be interpreted as $Cmcm$ space group violating reflections but are traces of the diffuse halos around specific reflections in adjacent layers (Figs. 6–9). All observations of diffuse scattering described in the literature and in this study point to structural $c/2$ defects. For correlated $c/2$ shifts Campbell and Cheetham (2002) have developed a strongly simplified model where the defect concentration (p_0) is related to the average diffuse intensity in $l = 2n + 1$ layers by a factor of $4p_0 (1 - p_0)$ whereas the intensity of the Bragg reflections in the corresponding layers decreases by $(1 - 2p_0)^2$. However, the diffuse intensity is not homogeneous in the $l = 2n + 1$ layers but enhanced in the form of halos around specific reflections which is related to the size and spatial correlation of the $c/2$ shifted

domains. No attempts have been made for a quantitative interpretation of diffuse-scattering features (e.g., Weber and Bürgi 2002) in mordenite.

Open questions

After we demonstrated in this study that two mordenite crystals with tetrahedral A1 concentrations of 16 (natural) and 12.5% (synthetic), respectively, have both $c/2$ shifted B domain defect concentrations of only ca. 3%, the concentration of B domains derived from powder Rietveld refinements (Campbell and Cheetham 2002; Rudolf and Garcés 1994) cannot be used as an indicator for the framework Al concentration. Other parameters related to the concentration of this type of defect have to be considered.

Natural modenities (small port) and the synthetic mordenite (large port) investigated by us show the same qualitative diffuse scattering features and $c/2$ defects. It remains enigmatic why natural mordenites show small port behavior.

Although $c/2$ defects are expected to cause diffuse scattering within reciprocal layers with $l = 2n + 1$, the inhomogeneous distribution of diffuse scattering has not yet been interpreted on a quantitative level. Thus the size and the spatial correlation of the intercalated B domains remain unknown.

The true symmetry of mordenite (Meier 1961; Gramlich-Meier 1981) remains controversial. Due to the strong $Cmcm$ pseudosymmetry of the average structure we can neither reject nor support the microtwin model of Gramlich-Meier (1981).

REFERENCES CITED

Akizuki, M., Kudoh, Y., and Nakamura, S. (1999) Growth texture and symmetry of heulandite-Ca from Poona, India. Canadian Mineralogist, 37, 1307–1312.
Alberti, A. (1997) Location of Brønsted sites in mordenite. Zeolites, 19, 411–415.
Alberti, A. and Gottardi, G. (1988) The determination of the Al-content in the tetrahedra of framework silicates. Zeitschrift für Kristallographie, 184, 49–61.
Alberti, A., Davoli, P., and Vezzalini, G. (1986) The crystal structure refinement of a natural mordenite. Zeitschrift für Kristallographie, 175, 249–256.
Armbruster, T. and Gunter, M.E. (2001) Crystal structures of natural zeolites. In D.L. Bish and D.W. Ming, Eds., Reviews in Mineralogy and Geochemistry, 45, Natural Zeolites: Occurence, Properties, Use, p. 1–67. Mineralogical Society of America, Washington, D.C.
Calzaferri, G., Brühwiler, D., Megelski S., Pfenniger M., Pauchard, M., Hennessy, Maas, H., Devaux, A., and Graf, U. (2000) Playing with dye molecules at the inner and outer surface of zeolite L. Solid State Sciences, 2, 421–447.
Campbell, B.J. and Cheetham, A.K. (2002) Linear framework defects in zeolite-mordenite. Journal of Physical Chemistry B, 106, 57–62.
Enraf-Nonius (1983) Structure determination package (SDP). Enraf Nonius, Delft, Netherlands.
Gramlich-Meier, R. (1981) Strukturparameter in Zeoliten der Mordenitfamilie. Diss. ETH, Nr. 6760.
Hamidi, F., Pamba, M., Bengueddach, A., Di Renzo, F., and Fajula, F. (2001) Factors affecting composition and morphology of mordenite. In A. Galarnau, F. Di Renzo, F. Faujula, and J. Vedrine, Eds., Studies in Surface Science and Catalysis 135, Zeolites and Mesoporous Materials at the Dawn of the 21st Century, abstract on p. 334, full paper on CD-ROM.
Itabashi, K., Fukushima, T., and Igawa, K. (1986) Synthesis and characteristic properties of siliceous mordenite. Zeolites, 6, 30–34.
Ito, M. and Saito, Y. (1985) The crystal structure of ion-exchanged mordenite. Bulletin of the Chemical Society of Japan, 58, 3035–3036.
Johnson, C.K. (1970) The effect of thermal motion on interatomic distances and

angles. In F.R. Ahmed, Ed., Crystallographic Computing, Munksgaard, Copenhagen, p. 220–226.

Jones, J.B. (1968) Al-O and Si-O tetrahedral distances in aluminosilicate framework structures. Acta Crystallographica B24, 355–358.

Kerr, I.S. (1963) Possible structures related to mordenite. Nature, 197, 1194–1195.

Lilis, R. (1981) Fibrous zeolites and endemic mesothelioma in Cappadocia, Turkey. Journal of Occupational Medicine, 23, 548–550.

Meier, W.M. (1961) The crystal structure of mordenite. Zeitschrift für Kristallographie, 115, 439–450.

——— (1978) Constituent sheets in the zeolites frameworks of the mordenite group. In L.B. Sand and F.A. Mumpton, Eds., Natural Zeolites, Occurrence, Properties, Use, p. 99–104.

Meier, W.M., Meier, R., and Gramlich, V. (1978) Mordenite: Interpretation of a superposed structure. Zeitschrift für Kristallographie, 147, 329.

Mortier, W.J., Pluth, J.J., and Smith, J.V. (1975) Positions of cations and molecules in zeolites with the mordenite-type framework; II Dehydrated hydrogen-ptilolite. Materials Research Bulletin, 10, 1319–1326.

——— (1978) Positions of cations and molecules in zeolites with the mordenite-type framework; IV Dehydrated and rehydrated K-exchanged ptilolite. In L.B. Sand and F.A. Mumpton, Eds., Natural Zeolites, Occurrence, Properties, Use, p. 53–76.

Oxford Diffraction (2001) Xcalibur System, User Manual, CrysAlis Software Package. Version 1.169. Oxfordshire, U.K.

Passaglia, E. (1975) The crystal chemistry of mordenites. Contributions to Mineralogy and Petrology, 50, 65–77.

Raatz, F., Marcilly, C., and Freund, E. (1985) Comparison between small port and large port mordenites. Zeolites, 5, 329–333.

Rudolf, P.R. and Garcés J.M. (1994) Rietveld refinement of several structural models for mordenite that account for differences in X-ray powder pattern. Zeolites, 14, 137–146.

Sand, L.B. (1968) Synthesis of large-port and small port mordenites. Molecular Sieves, Conference Papers, Meeting Date 1967, 71–77. Society of Chemical Industry, London.

Sanders, J.V. (1985) Crystallographic faulting in the mordenite group zeolites. Zeolites, 5, 81–89.

Sano, T., Wakabayashi, S., Oumi, Y., and Uozumi, T. (2001) Synthesis of large mordenite crystals in the presence of aliphatic alcohol. Microporous and Mesoporous Materials, 46, 67–74.

Sheldrick, G.M. (1997) SHELX-97. University of Göttingen, Germany.

Sherman, J.D. and Bennett, J.M. (1973) Framework structures related to the zeolites mordenite. In W.M. Meier and J.B. Uytterhoeven, Eds., Molecular Sieves, p. 52–65. ACS monograph, American Chemical Society, Washington, D.C.

Shiokawa, K., Ito, M., and Itabashi K. (1989) Crystal structure of synthetic mordenite. Zeolites, 9, 170–176.

Simoncic, P. and Armbruster, T. (2002) Synthesis of mordenite single crystals for dye incorporation. Zeolite '02, 6th international conference on the occurences, properties, and utilization of natural zeolites, Thessaloniki. In P. Misaelides, Ed., Book of Abstracts, 336.

Song, S.G. (1999) Crystal defects of mordenite crystals. Journal of Materials Research, 14, 2616–2620.

Stephenson, D.J., Fairchild, C.I., Buchan, R.M., and Dakins, M.E. (1999) A fiber characterization of the natural zeolite, mordenite: A potential inhalation health hazard. Aerosol Science and Technology, 30, 467–476.

Tarasevich, Y.I., Krysenko, D.A., and Polyakov, V.E. (2002) Selectivity of low- and high-silica clinoptilolites with respect to alkali and alkaline earth metal cations. Colloid Journal, 64, 759–764.

Terasaki, O., Yamazaki, K., Thomas, J.M., Ohsuna, T., Watanabe, D., Sanders, J.V., and Barry, J.C. (1988) The incorporation of selenium into the channels of mordenite: An electron microscopic study. Journal of Solid State Chemistry, 77, 72–83.

Warzywoda, J., Dixon, A.G., Thompson, R.W., and Sacco, A. Jr. (1995) Synthesis and control of the size of large mordenite crystals using porous silica substrates. Journal of Materials Chemistry, 5, 1019–1025.

Warzywoda, J., Dixon, A.G., Thompson, R.W., Sacco, A. Jr., and Suib, S.L. (1996) The role of the dissolution of silicic acid powders in aluminosilicate synthesis mixtures in the crystallization of large mordenite crystals. Zeolites, 16, 125–137.

Weber, T. and Bürgi, H.B. (2002) Determination of disordered crystal structures using evolutionary algorithms in combination with Monte Carlo Methods. Acta Crystallographica, A58, 526–540.